DOI: 10.1002/ ((please add manuscript number))
Article type: Full Paper

Highly Controlled Zigzag Perovskite Nanocrystals Enabled by Dipole-induced Self-Assembly of Nanocubes for Low-threshold Amplified Spontaneous Emission and Lasing

Chengxi Zhang, Jiayi Chen, Lyudmila Turyanska, Junhui Wang, Weihua Wang, Lin Wang, Lingmei Kong, Kaifeng Wu, Jisong Yao, Hongbin Yao, Zhiwen Yang, Wanwan Li, Yehonadav Bekenstein, Yue Wang,* Guohua Jia,* and Xuyong Yang*

Dr. C. Zhang, Dr. L. Wang, L. Kong, Prof. X. Yang
Key Laboratory of Advanced Display and System Applications of Ministry of Education, Shanghai University, 149 Yanchang Road, Shanghai 200072, China
E-mail: yangxy@shu.edu.cn

Dr. J. Chen, Prof. G. Jia[1,2]
[1]School of Molecular and Life Sciences, Curtin University, GPO Box U1987, Perth, WA 6845, Australia
[2]Key Lab for Special Functional Materials, Ministry of Education, National and Local Joint Engineering Research Center for High-Efficiency Display and Lighting Technology, School of Materials Science and Engineering, and Collaborative Innovation Center of Nano Functional Materials and Applications, Henan University, Kaifeng 475004, China
E-mail: guohua.jia@curtin.edu.au

Dr. L. Turyanska
Faculty of Engineering, University of Nottingham, Nottingham NG7 2RD, UK

J. Wang, Prof. K. Wu
State Key Laboratory of Molecular Reaction Dynamics and Collaborative Innovation Center of Chemistry for Energy Materials, Dalian Institute of Chemical Physics, Chinese Academy of Sciences, Dalian, China

W. Wang, Prof. Y. Wang
MIIT Key Laboratory of Advanced Display Materials and Devices, Institute of Optoelectronics & Nanomaterials, College of Materials Science and Engineering, Nanjing University of Science and Technology, Nanjing, 210094, China
E-mail: ywang@njust.edu.cn

J. Yao, Prof. H. Yao
Hefei National Laboratory for Physical Sciences at the Microscale, University of Science and Technology of China, Hefei, Anhui 230026, China

Dr. Z. Yang, Prof. W. Li
State Key Lab of Metal Matrix Composites, School of Materials Science and Engineering, Shanghai Jiao Tong University, 800 Dongchuan Road, Shanghai 200240, China

Prof. Y. Bekenstein
Department of Materials Science and Engineering, Technion – Israel Institute of Technology, Haifa, 3200003

Abstract: Self-assembly of nanocrystals into controlled structures while uncompromising their properties is one of the key steps in optoelectronic device fabrication. Herein, we demonstrate zigzag $CsPbBr_3$ perovskite nanocrystals with a precise number of components with nanocube morphology can be successfully obtained through a dipole-induced self-assembly process. The addition of a trace amount of DI water facilitates the transfer from $CsPbBr_3$ nanocubes to intermediates of $CsPb_2Br_5$ and $Cs_3In_2Br_9$, which then fastly release reaction monomers leading to further homogenous nucleation of $CsPbBr_3$ nanocubes, followed by the formation of zigzag $CsPbBr_3$ nanocrystals through a dipole-induced self-assembly process. Dipole moment along <110> axis is found to be the driving force for the assembly of nanocubes into zigzag nanocrystals. The zigzag $CsPbBr_3$ nanocrystals exhibit desirable optical properties comparable to their nanocube counterparts and offer advantages for amplified spontaneous emission (ASE) and lasing applications with low pump thresholds of 3.1 μJ/cm^2 and 6.02 μJ/cm^2, respectively. This work not only develops a strategy for producing highly controlled zigzag perovskite nanocrystals and provides insights on the dipole-induced self-assembly mechanisms, but also opens an avenue for their application in lasing.

Keywords: zigzag perovskite nanocrystals, dipole-induced self-assembly, optical properties, amplified spontaneous emission, lasing

1. Introduction

Metal-halide perovskite nanocrystals have attracted tremendous attention due to their superior properties, including narrow emission linewidth, high photoluminescence quantum yield, high defect tolerance, high optical absorption coefficient, and long carrier diffusion length.[1-5] Significant advancements have been made in developing their synthetic methods and optimizing their surface chemistry for retaining their stability while keeping their optical and photovoltaic properties uncompromised.[6-16] However, unlike widely established traditional semiconductors such as chalcogenides and metal oxides, the control of the growth kinetics of perovskite nanocrystals is very difficult because of their highly ionic nature and fast formation processes.[17-20] This presents challenges for expanding the research on the development of anisotropic and self-assembled perovskite structures. So far, only limited success has been achieved in the morphology control such as nanorods and nanosheets for single perovskite particles,[9, 21] for example B-site cation exchange process was used to grow anisotropic $CsPbBr_3$ nanostructures.[22] However the challenge of precise control of the size and shape of the perovskite nanostructures remains to be addressed and the research on self-assembly of perovskite nanocrystals is still in its infancy. There is a strong need for alternative materials for scalable fabrication of lasing devices using solution processing. To date, the low threshold lasing was achieved with structures produced using chemical vapor deposition (CVD) method,[23] however these devices require complex growth and processing. Anisotropic perovskites could offer promising opportunities for scalable low-cost lasing applications.

In this letter, we report on the formation of zigzag-shaped $CsPbBr_3$ perovskite nanocrystals with a precisely controlled number (n = 2, 3…) of nanocube components, achieved through a dipole-induced self-assembly process from perovskite nanocubes. The addition of a trace amount of water triggers the rapid conversion of the perovskite nanocubes into intermediate monomers, which provide the feeding stock for the homogenous nucleation of perovskite nanocubes. The dipole along the <110> direction induces the self-assembly of these perovskite

nanocubes, producing zigzag perovskite nanocrystals. This unique approach enables the precise control of the anisotropic entities of zigzag $CsPbBr_3$ perovskite nanocrystals while does not compromise their optical properties and stability. Remarkably, the amplified spontaneous emission (ASE) applications of zigzag $CsPbBr_3$ have been demonstrated, in which an ultralow threshold of 3.1 μJ/cm^2 was achieved. Impressively, the integration of the zigzag $CsPbBr_3$ nanocrystals into whispering gallery mode (WGM) cavity enabled the lasing output with a threshold of 6.02 μJ/cm^2. Our synthetic approach shows that the morphological properties of the perovskite nanocrystals can be engineered by the regulation of dipole moments. These zigzag nanocrystals with high quantum yields demonstrated the great potential of for lasing applications and could be advantageous for other optoelectronic devices.

2. Results and Discussion

$CsPbBr_3$ nanocube seeds were synthesized firstly according to a literature method previously reported by our group[5] and then were used for the growth of zigzag $CsPbBr_3$ nanocrystals. The as-synthesized $CsPbBr_3$ nanocrystals are uniform cubic structured nanocubes with an average size of ~ 13.4 ± 1.3 nm (Supplementary Information, SI2, **Figure S1**). $In(OAm)_3$ was used as a conversion agent to initiate the transfer from $CsPbBr_3$ nanocube seeds into intermediates of $Cs_3In_2Br_9$ and $CsPb_2Br_5$.[5] To facilitate this transfer process, a small amount of deionized (DI) water, ca 100 μL, was intentionally added to the $In(OAm)_3$ solution, and then mixed sequentially with dodecane and $CsPbBr_3$ nanocube seeds, and finally the mixture immediately produced a transparent solution. Zigzag-shaped $CsPbBr_3$ nanocrystals were formed after the mixture has been evolved for 15 min at 95 ^oC (**Figure 1A**).

High-angle annular dark-field scanning transmission electron microscopy (HAADF-STEM) (**Figure 1A**) and high-resolution transmission electron microscopy (HRTEM) (**Figure 1B**) were used to analyze the morphology of the zigzag $CsPbBr_3$ nanocrystals. The lattice spacing of the crystal faces perpendicular to the edge was ~ 0.58 nm, which corresponds to

(100) and (010) planes of the cubic phase $CsPbBr_3$.[24] This assignment is further supported by the consistence between the fast Fourier transform (FFT) patterns (**Figure 1C**) and the simulated electron diffraction (ED) patterns (**Figure 1D** and Supplementary Information, **SI2, Figure S2**). Diffraction peaks in the X-ray diffraction (XRD) pattern of the zigzag $CsPbBr_3$ nanocrystal films confirmed their crystal structure is cubic (**Figure S2D**). Elemental map elemental line scans of individual nanoparticles confirm the uniform distribution of Cs, Pb, Br throughout the zigzag $CsPbBr_3$ nanocrystal (**Figure 1E,** Supplementary Information SI2, **Figure S2E**). No detectable In signal was recorded in the element maps, confirming the complete conversion of the $Cs_3In_2Br_9$ intermediates into zigzag $CsPbBr_3$ nanocrystals.

To gain better control of the zigzag $CsPbBr_3$ nanocrystals, especially to produce zigzag nanocrystals with an exact number n (n=2, 3, 4, 5…) of nanocube components, the growth process of the zigzag $CsPbBr_3$ nanocrystals was performed at a variety of temperatures such as 95 °C, 105 °C and 125 °C with a heating period of 6 min for each temperature (Supplementary Information SI2, **Figure S3**). The zigzag $CsPbBr_3$ nanocrystals were formed at T = 95 and 105 °C, while a mixture of rod-like and sheet-like nanocrystals were also formed at T = 125 °C (**Figure S3**). We note, that there is no indication of any merging between the neighbouring zigzag structures, which remain individual within a perovskite layer. The step-by-step growth of the zigzag structure was observed by recording TEM images at different stages of this process. Just as the temperature of the reaction system reached 95 °C and 105 °C (t = 0 min), the zigzag nanocrystals with the number of cubes n =2 – 3 were formed. With increasing the reaction time to t = 6 min, the number of nanocubes in the zigzag nanocrystals increases to n = 4. Further increase of time to t = 15 min does not lead to further increase of n, which is likely because there are no remaining perovskite seeds in the reaction system for the growth of zigzag nanocrystals. To verify our hypothesis, we increased the volume of the perovskite seeds from V_{seed} = 6 mL to 7 mL. In this case, zigzag nanocrystals with n > *4* (Supplementary Information, SI2, **Figure S4**) were formed. Further increasing V_{seed} did not yield zigzag nanocrystals with a

larger *n* since the perovskite seeds tend to incompletely decompose with an insufficient amount of $In(OAm)_3$, which can be confirmed by the green photoluminescence of the reaction mixture. These studies demonstrated that the zigzag $CsPbBr_3$ perovskite nanocrystals with controlled *n* values can be accomplished through manipulating growth conditions. As demonstrated in the formed zigzag nanocrystals with the thickness of 50 nm, the zigzag nanocrystals do not evolve toward belts or nanosheets (see the red circles in **Figure 1E-H** and Supplementary Information SI2, **Figure S5**). We note, that while semiconductor zigzags (PbS and PbSe) were produced through the oriented attachment of nanoparticles, their growth was facilitated using surfactants and regulation of the reaction temperature.[25-26] This method cannot be applied to prepare zigzag perovskite nanocrystals due to instability of perovskite nanocube components.[27] Hence our approach provides a robust method for growth of zigzag perovskite nanocrystals.

To understand the growth mechanism of zigzag $CsPbBr_3$ nanocrystals, aliquots were taken and analysed at different stages of the reaction process (Supplementary Information, SI3, **Figures S6-S7**). Following the addition of $In(OAm)_3$ into the solution of $CsPbBr_3$ seeds, Pb^{2+} was replaced by In^{3+}cations and produced $Cs_3In_3Br_9$ due to the higher binding energy of Br−In (409 ± 10 kJ/mol) compared to that of Br−Pb (248.5 ± 14.6 kJ/mol).[28] The increase of lead cation concentration in the reaction mixture promotes the transformation of $CsPbBr_3$ to $CsPb_2Br_5$,[29] as evidenced by the colour change of the reaction solution from bright green to colourless and then to transparent. The presence of these intermediates such as $Cs_3In_3Br_9$ and $CsPb_2Br_5$ were confirmed by the TEM and XRD results (Supplementary Information, SI3, **Figure S8**),[5, 30] where the change in seed morphology from cubic to quasi-spherical was observed. As the reaction temperature increased to 60 ^oC, the colour of the solution gradually changed to milky white, with more regular pentagonal shaped particles being observed. Further increasing the transformation temperature to 95 ^oC produced regular polyhedral shaped nanoparticles, which then gradually transformed into zigzag nanocrystals with n = 2−3, and simultaneously, the colour of the solution became transparently yellow-green. Further increase

of the heating time to 15 min resulted in the formation of zigzag $CsPbBr_3$ nanocrystals with $n = 3-4$.

The change of the reaction products at different stages of the growth process was further confirmed by XRD studies. Following the addition of $In(OAm)_3$, the intensity of the diffraction peaks corresponding to $CsPbBr_3$ seeds decreased gradually, while the diffraction peaks of intermediates appeared (Supplementary Information, SI3, **Figure S8**). Upon reaching $T = 95\ ^oC$, the diffraction peaks corresponding to (100), (110) and (200) planes of perovskite nanocrystals are observed (**Figure S8**). The intensity of the (110) peak is higher in zigzag $CsPbBr_3$ nanocrystals compared to that in $CsPbBr_3$ nanocubes. These results confirm that the intermediates are completely decomposed and transformed into zigzag nanocrystals connected along the <110> direction, as confirmed by the HRTEM studies (**Figure 1B**).

The evolution of the compositions of both the intermediates and zigzag nanocrystals was studied by X-ray photoelectron spectroscopy (XPS) (Supplementary Information, SI4). The Pb 4f and Br 3d peaks shift to higher binding energies as the reaction temperature increases from 30 ^oC to 60 ^oC, which corresponds to the transformation from $CsPbBr_3$ to $CsPb_2Br_5$. The Br 3d peaks shift to higher binding energies, as expected for intermediate $Cs_3In_2Br_9$. At $T = 95\ ^oC$, the zigzag nanocrystals start to form, and the position of the Pb 4f and Br 3d peaks is comparable to that of the nanocubes. No In 3d peak was observed in the XPS spectra of zigzag $CsPbBr_3$ nanocrystals, confirming the absence of In in these structures (**Figure 1I** and **Figure S2**).

To elucidate the role of DI water in the growth of zigzag $CsPbBr_3$ nanocrystals, we performed control experiments by conducting the synthesis in the presence of and in the absence of a trace amount of DI water (Supplementary Information, SI3, **Figure S9**). In the trace amount of water-treated $In(OAm)_3$ solution, $CsPbBr_3$ nanocube seeds decompose rapidly into intermediates within 1 min. However, it takes more than one hour for $CsPbBr_3$ nanocubes to decompose in the absence of DI water (**Figure S9**). When the water content was 30 µL, the product with the morphology of NRs was obtained while zigzag-shaped nanocrystals appeared

when the water content was increased (the optimum amount of DI water is 100 μL). However, excess amount of the DI water led to a mixture containing zigzag and other shaped nanocrystals (Supplementary Information, SI3, **Figure S10**). We envisaged that a trace amount of water in the reaction solution could trigger the fast conversion from $CsPbBr_3$ nanocube seeds to the intermediates of $CsPb_2Br_5$ and $Cs_3In_2Br_9$ with quasi-spherical morphology (Supplementary Information, SI3, **Figure S11**), which then provide sufficient feeding stock for homogenous nucleation of $CsPbBr_3$ nanocubes following by the formation of zigzag $CsPbBr_3$ nanocrystals *via* self-assembly (**Figure S11**). In contrast, in the reaction that does not involve any water, rod-like intermediates were produced due to the anisotropic growth of perovskite nanocrystals. In this case, the rate of the release of reaction monomers from the intermediates of $CsPb_2Br_5$ and $Cs_3In_2Br_9$ is much slower, which ensures continuous feeding of the reaction monomers that favorites anisotropic growth of $CsPbBr_3$ nanorods (**Figure S11**). A certain amount of DI Water can induce the decomposition of pristine nanocrystals at a certain rate and the release of intermediates from monomers gradually, resulting in the formation of zigzag perovskite nanocrystals. However, in the absence of DI water, the rate of the transformation of intermediates and the release of monomers become much slower, leading to the formation of the rod-shape nanocrystals. In our work, we use a mixture of OA/OLA as capping ligands, however we envisage that this strategy can be transferred onto nanocubes capped with different capping molecules.

It is well established that the inherent anisotropy of crystal structure is the driving force for the growth of anisotropic nanocrystals.[21, 31-32] However, cubic structured $CsPbBr_3$ nanocubes have isotropic crystal lattices, it is counter-intuitive that such isotropic nanoparticles attach along the specific direction of <110> of the cubic lattices of $CsPbBr_3$ to form zigzag structures. Hence, we propose that dipole interactions could be the driving force that directs the self-assembly of individual $CsPbBr_3$ nanocubes into zigzag $CsPbBr_3$ nanocrystals.

Schematic models (**Figure 2**) indicate the origin of a dipole moment for cubic structured $CsPbBr_3$ nanocrystals. The nanocube is terminated by six {100}, twelve {110} and eight {111} facets. Among them, {100} facets are non-polar, as they have two terminated surfaces, CsBr and $PbBr_2$, both of which are neutral (the net charge is zero). The {110} facets are either positively charged or negatively charged (i.e., polar facets), as $(Br_2)^{2-}$ and $(CsPbBr)^{2+}$ surfaces presented alternatively along the <110> direction in a cubic $CsPbBr_3$. The {111} facets are terminated by either $(Pb)^{2+}$ or $(CsBr_3)^{2-}$ so they could also be polar.[33] Therefore, the electric charge distribution within a $CsPbBr_3$ nanocrystal is dependent on the arrangement of the polar facets of both {110} and {111} facets. To maintain the electric neutrality and the chemical stoichiometry, the net number of charges for all polar surfaces of a $CsPbBr_3$ nanocrystal should be zero. The self-assembly of $CsPbBr_3$ nanocubes starts at elevated temperatures such as 95 ^oC because a high temperature makes the surface ligands more liable so these ligands could be partially stripped off. We assume $CsPbBr_3$ nanocrystals are ideal cubic, and simplify this case as {110} facets could be terminated by 6 $(Br_2)^{2-}$ and 6 $(CsPbBr)^{2+}$ layers, and similarly, the terminated {111} facets contain 4 $(Pb)^{2+}$ and 4 $(CsBr_3)^{2-}$ layers,[25] with a random arrangement of these negative or positive charged layers so the whole nanoparticle which has central symmetry can possess zero net dipole moment. Asymmetric distribution of {110} facets will result in a dipole moment along <100>, <110> or <111> directions, providing the driving force for the oriented attachment of cubic structured $CsPbBr_3$ nanocrystals that leads to the formation of zigzag structures. To simplify the analysis of the origin of dipole moments, the dipole moments induced by {110} and {111} facets will be considered separately.

The distribution of negative and positive facets (**Figure 2B-C**) can be described using probabilities ratios of different dipole moment directions; that attributed to {110} facets is 0:<100>:<110>:<111> = 8:25:52:8, and that for {111} is 0:<100>:<110>:<111> = 4:15:12:4 (Supporting information, SI1). The arrangement of polar facets also determines the dipole moment magnitudes, so the ratio values of dipole moment along different <hkl> axes should be

$<100>_{large}$:$<100>_{small}$:$<110>_{large}$: $<110>_{small}$:<111> = 2:1:$\sqrt{2}$:1:$\sqrt{3}$ for dipole moment generated by {110} facets, while it is $<100>_{large}$:$<100>_{small}$:<110>:<111> = 2:1:1:$\sqrt{2}$ for {111} facets. In the prediction, the majority (~ 54%) of the cubic nanocrystals are expected to have permanent dipole moment along <110> axis with a sufficient magnitude to drive the nanocubes to form zigzag structures, which is consistent with our TEM results. For the $CsPbBr_3$ nanocrystal with non-ideal nanocube structure, a slightly elongated rectangular prism can be formed (**Figure 2D**). Under such circumstances, both their length and the net of charges of {110} facets are unequal, inducing a slight shift of dipole moment direction pointing between <110> and <100>. Thus, the attachment of these elongated rectangular prisms will not occur along <110> direction as previously observed for the cubic structured $CsPbBr_3$ nanocubes. Instead, they will attach along a direction between <110> and <100> and form partial overlap on (100) facets of these rectangular prisms, and finally produce asymmetrical zigzag structures (**Figure 2E**).

It is well known that the change of the nanocrystal shape may significantly affect their optical properties. For the $CsPbBr_3$ nanocubes, the PL peak position is at λ_{PL} = 514 nm with a full-width at half-maximum (FWHM) of 20 nm and a photoluminescence quantum yield (PLQY) = 88% and an average PL decay lifetime (τ_{ave}) is 16 ns (**Figures 3A-B** and Supplementary Information SI5, **Table S1**). When nanocubes are transformed into zigzag nanocrystals with different *n* numbers, the PL peak and FWHM remain comparable to those of $CsPbBr_3$ nanocubes. The PLQY of the zigzag nanocrystals maintains a high value of over 82%. A small decrease (6%) of the PLQY can be attributed to additional purification process conducted for zigzag nanocrystals. This subtle decrease is negligible considering the surface area of zigzag perovskite nanocrystals is significantly increased compared with that of each individual nanocube component. This result suggests that there is no PL quenching during the particle self-assembly and no defects were introduced into the zigzag nanocrystals during their formation. In contrast, complex perovskite nanocrystals of other morphology reported in the

previous literature showed a significant decrease of their PLQY due to increased surface and defects.[9, 14, 22, 27] However, a longer luminescence lifetime τ_{ave} = 23 ns is observed for the zigzag perovskite nanocrystals due to the reduced number of nonradiative recombination centers, which is consistent with the induced percentage of τ_1 lifetime (A_1). This clearly demonstrated that precisely controlled zigzag $CsPbBr_3$ perovskite nanocrystals with n = 2, 3, 4 were successfully obtained without compromising their optical properties.

Temperature-dependent PL measurements were used to probe the presence of defect states (**Figure 3C-E** and Supplementary information, SI5, **Figure S14**). For both nanocube and zigzag samples, a blue-shift of the PL peak position accompanied by the broadening of the optical line is observed in the temperature range from 80 to 300 K, as expected for metal halide perovskite nanocrystals.[3, 5] The PL peak blueshift by 42 meV for freshly synthesized $CsPbBr_3$ nanocubes, and by 39 meV for n = 4 zigzags stored for three months in fridge at T = 5 °C. The observed similarity of the T-dependence of the optical bandgap indicates that exciton confinement is not affected by the assembly of nanocube into zigzags. The decrease of the integrated PL intensity with increasing T originated from a thermally activated nonradiative recombination processes[34] and a similar exciton-binding energy between nanocubes and zigzags (nanocube: E_b = 67.64 meV *vs.* zigzag: E_b = 62.27 meV) was observed for all the studied samples (Figure 3D). The FWHM (Figure 3E) of the n =4 zigzag $CsPbBr_3$ is 102 meV at room temperature, being slightly broader than that for the $CsPbBr_3$ nanocubes (FWHM = 85 meV) results from a small decrease of the strength of exciton-phonon coupling for the zigzag $CsPbBr_3$ nanocrystals.[3, 35-37] Of particular interest for potential applications is the stability of the colloidal suspension of nanocrystals. The zigzag $CsPbBr_3$ nanocrystals retained their optical properties for at least 3 months (Supplementary information, SI5, **Figure S15**), making them promising candidates for optoelectronic applications.

We explore the potential of zigzag $CsPbBr_3$ nanocrystals for ASE applications. The zigzag $CsPbBr_3$ nanocrystals were spin-coated on glass substrate under inert atmosphere to form close-

packed thin films. The device was pumped by the femtosecond lasing pulses (λ_{pump} = 400 nm, 100 fs, 1 kHz) in standard stripe pumping configuration (SPC). The emission spectra were recorded as a function of the pump energy (E_{pump}), (**Figure 4**). For low E_{pump} < 2.8 μJ/cm^2, we observe an emission spectrum centred at λ = 522 nm with FWHM = 20 nm. With increasing E_{pump}, a narrow peak appears at λ ~ 534 nm with FWHM = 4.4 nm. The threshold behavior with a steep rise in intensity of the peak at λ = 534 nm is characteristic for ASE. Also, the dependence of the integrated intensity of the sharp peak (at λ = 534 nm) on E_{pump} exhibits a super-linear behavior, confirming the observation of ASE phenomenon in these zigzag $CsPbBr_3$. The ASE threshold is estimated to be at E_{pump} = 3.1 μJ/cm^2, which is among the lowest values reported for colloidal nanocrystal-based ASE to date.[38-40] Such a low ASE energy threshold can be explained by the dense packing in the solid film and low defect state density in zigzag nanocrystals. Importantly, the excellent stability of the ASE from the zigzag $CsPbBr_3$ is achieved upon uninterrupted femtosecond laser irradiation. At least, ~ 80% of its initial intensity value is retained after 6.0 h of femtosecond laser radiation (2.16×10^7 laser pulses with E_{pump} = 5.20 μJ/cm^2).

The low ASE energy threshold and long-term photostability demonstrated for zigzag nanocrystals can be employed to realize lasing, when an appropriate cavity resonator is used.[41] Colloidal nature of the zigzag $CsPbBr_3$ nanocrystals enable their integrations into various cavities, such as WGM resonator. As a demonstration, the close-packed zigzag $CsPbBr_3$ nanocrystals solid film (n = 4) was deposited onto the surface of SiO_2 microfiber to form a WGM cavity and the femtosecond laser pulses (400 nm, 100 fs, 1 kHz) were used. We note, that full coverage of nanostructures is beneficial for lasing applications aiming to achieve higher optical gain and optimized lasing threshold. Broad photoluminescence peak is observed for the low E_{pump} below the threshold value. For E_{pump} above the laser threshold, a series of evenly-spaced peaks emerged at λ ~ 534 nm (**Figure 5A-B**). A super-linear increase of the integrated

intensity of these peaks with increasing E_{pump} confirms the occurrence of WGM lasing action. The FWHM of the lasing peaks is 0.2 nm, corresponding Q-factor of about 2700 (**Figure 5C**). Benefitting from the high PLQY and long-term stability of optical properties of zigzag $CsPbBr_3$ nanocrystals, the laser threshold in this experiment is estimated to be at 6.02 μJ/cm^2 (**Figure 5D**), the low lasing threshold can be attributed to the superior gain properties and the high Q-factor of the nanocrystal-WGM system.

The polarization of lasing emissions from the zigzag $CsPbBr_3$ nanocrystals and SiO_2 microfiber was also measured, the intensity was recorded as a function of the linear polarizer angle at a fixed pump fluence (E_{pump} = 7.52 μJ/cm^2). The obtained experimental data can be fitted with a quadratic sine function (**Figure 5E**), demonstrating that the transverse-magnetic lasing mode with magnetic field polarized predominantly in *y*-direction. The factor of the polarization state, R, was calculated using the following expression: $R = (I_{\parallel} - I_{\perp})/(I_{\parallel} + I_{\perp})$, where $I_{\parallel}$ and $I_{\perp}$ correspond to the lasing intensities parallel and perpendicular to the *x*-axis, respectively.[42-44] We obtained R = 0.80 from the nanocrystal-fiber system, which further indicates the high performance of the laser emission. This value is higher than the polarization measured from $CsPbBr_3$ nanowires and nanoplates[45-46]

3. Conclusion

In conclusion, we have developed a strategy of dipole-induced self-assembly for the synthesis of zigzag $CsPbBr_3$ perovskite nanocrystals with a precisely controlled number of nanocube components. The formed zigzag $CsPbBr_3$ nanocrystals exhibit optical properties comparable to those of the nanocube seeds with high PLQYs and long-term storage stability. We demonstrated ASE and lasing application for these zigzag $CsPbBr_3$ nanocrystals with the lowest energy threshold of 3.1 μJ/cm^2 and 6.02 μJ/cm^2, respectively, to date. This study not only provides significant insights into the growth mechanisms that underpin the formation of zigzag $CsPbBr_3$ perovskite nanocrystals but also opens up exciting prospects for their

applications in optoelectronics, especially in lasing.

4. Experimental Section

Preparation of oleylammonium bromide (OAmBr): To prepare the OAmBr precursor, 100 mL ethanol, 12.5 mL oleylamine (OLA, Sigma-Aldrich, 90%) and 10 mL of hydrobromic acid (HBr, Sigma-Aldrich, 48% aqueous solution) were mixed under nitrogen flow in a 250 mL round-bottomed flask at T = 0 °C for 12 h with continuous stirring. A pale brown solution was obtained and dried in a rotary evaporator at T = 50 °C. The obtained powder was recrystallized using diethyl ether (100 mL, three times) and the white OAmBr powder was collected and dried at T = 40 °C in a vacuum oven for 3 h.

Preparation of In(OAm)$_3$: 3 mmol indium (III) acetate (In(OAc)$_3$, Alfa Aesar, 99.99%), 6 mL OLA and 30 mL dodecane were mixed in a 50 mL three-neck flask and degassed under nitrogen flow for 20 min at T = 80 °C. After the complete dissolution of In(OAc)$_3$, the In(OAm)$_3$ solution was cooled down to room temperature.

CsPbBr$_3$ nanocubes precursor and CsPbBr$_3$ nanocubes: 1.13 mmol PbBr$_2$ (Sigma-Aldrich, 98%), 1.13 mmol OAmBr and 30 mL dodecane were added into a 50 mL three-neck flask. The mixture was degassed at T = 100 °C for 30 min under nitrogen protection. OA and OLA (3 mL, vacuum dried at 120 °C, respectively) were injected and the mixture was stirred at T = 120 °C for 30 min to form a clear solution. The temperature was further increase to T = 180 °C. The as-synthesized cesium stearate (CsSt, > 98%) precursor formed by dissolving 1.13 mmol CsSt with 3 mL dodecane at T = 150 °C for 30 min was quickly injected into the reaction solution. The yellow-green coloured solution was cooled down in an ice-water bath and stored in a fridge at 5 °C.

Synthesis of zigzag CsPbBr$_3$ nanocrystals: A synthetic protocol was optimized for the preparation of n = 4 zigzag CsPbBr$_3$ nanocrystals. For a typical synthesis, 6 mL In(OAm)$_3$ solution and 7 mL dodecane were mixed in a 50 mL centrifuge tube ultrasonic treatment for 5

min, then 100 μL deionized (DI) water (FST-PF-UP-1000L, Fu Instrument equipment) was added into the mixture and ultrasonicated for 15 min to form a transparent solution. 6 mL solution of $CsPbBr_3$ nanocubes was added to form a light-yellow solution, which then was transferred into a 50 mL three-neck flask under nitrogen flow. After the solution was heated to 60 °C for 10 min, a milky white solution was formed. The temperature was further increased to T = 95 °C and kept at this temperature for 20 min to produce zigzag nanocrystals. The golden yellow transparent mixture was cooled in an ice-water bath.

Purification: Crude solutions of $CsPbBr_3$ nanocubes or $CsPbBr_3$ nanocrystals were added to ethyl acetate with volume ratio of 1:3, and centrifuged for 3 min at 7800 rpm. The supernatant was discarded, and the precipitate was redispersed in hexane. The process was repeated twice.

Structural and chemical analysis: The transmission electron microscopy (TEM) images were obtained using a JEOL JEM-2100F transmission electron microscope operated at 200 kV. High-angle annular dark-field scanning (HAADF-STEM) images were recorded on FEI Tecnai G20 transmission electron microscope operated at 200 kV. X-ray diffraction patterns (XRD) were obtained using a Rigaku D/max 2500 diffractometer equipped with a rotating anode and a Cu Kα radiation source (λ = 0.15418 nm). X-ray photoelectron spectroscopy (XPS) measurements were carried out on a ULVAC-PHI 5000 VersaPr obe instrument with an achromatic Al Kα source (1486.6 eV) and a double pass cylindrical mirror analyzer.

Optical characterization: Absorption spectra were measured on a PerkinElmer Lambda 950 UV–vis–NIR spectrometer. The photoluminescence spectrum, fluorescence lifetime and absolute fluorescence quantum yield were measured using a photoluminescence spectrometer of FLS-1000 (Edinburgh Instruments) equipped with the ultrafast light source, integrating sphere and PMT-900 standard detector. Temperature-dependent PL measurements were measured by a static/transient fluorescence spectrometer (Edinburgh instruments; FLS 1000-stm), and the samples were drop-casted on silicon wafers and the temperature range from 80 K to 300 K was controlled by using a nitrogen cryostat. For ASE measurements, mode-locked

femtosecond laser was used as the pumping source with a repetition rate of 1 kHz, a pulse width of 100 fs at λ = 400 nm, and a cylindrical lens was used to obtain stripe geometry. A neutral density filter was placed between the laser and the sample to adjust the pumping intensity. The emission of the sample was collected using SR-750-D1 monochromator (ANDOR). For the lasing characterization, pulsed laser (400 nm, 100 fs, 1 kHz) was focused onto the sample using 20 X and 40 X objective lens. The signal was collected by a monochromator coupled with a charge-coupled device (CCD) and the real-color images were taken by a high-resolution camera.

Supporting Information

Supporting Information is available from the Wiley Online Library or from the author.

Acknowledgements

The authors acknowledge the financial support from the National Key Research and Development Program of China (2022YFE0200200), National Natural Science Foundation of China (62174104 and 52102182), Shanghai Science and Technology Committee (19010500600), China Postdoctoral Science Foundation (2020M680054, 2021T140440), the Australian Research Council (ARC) Future Fellowship Scheme (G.J., FT210100509) and the ARC Discovery Project Scheme (DP220101959).

Author Contributions

Chengxi Zhang, Jiayi Chen, Lyudmila Turyanska contributed equally to this work.

Conflict of Interest

The authors declare no conflict of interest.

Received: ((will be filled in by the editorial staff))

Revised: ((will be filled in by the editorial staff))

Published online: ((will be filled in by the editorial staff))

References:

[1] X. Liu, W. Xu, S. Bai, Y. Jin, J. Wang, R. H. Friend, F. Gao, *Nat. Mater.* **2021**, 20, 10.

[2] V. K. Ravi, S. Saikia, S. Yadav, V. V. Nawale, A. Nag, *ACS Energy Lett.* **2020**, 5, 1794.

[3] C. Zhang, S. Wang, X. Li, M. Yuan, L. Turyanska, X. Yang, *Adv. Funct. Mater.* **2020**, 30, 1910582.

[4] C. Zhang, J. Chen, S. Wang, L. Kong, S. W. Lewis, X. Yang, A. L. Rogach, G. Jia, *Adv. Mater.* **2020**, 32, 2002736.

[5] S. Wang, J. Yu, M. Zhang, D. Chen, C. Li, R. Chen, G. Jia, A. L. Rogach, X. Yang, *Nano Lett.* **2019**, 19, 6315.

[6] J. Shamsi, A. S. Urban, M. Imran, L. De Trizio, L. Manna, *Chem. Rev.* **2019**, 119, 3296.

[7] Q. A. Akkerman, V. D'Innocenzo, S. Accornero, A. Scarpellini, A. Petrozza, M. Prato, L. Manna, *J. Am. Chem. Soc.* **2015**, 137, 10276.

[8] D. Parobek, Y. Dong, T. Qiao, D. Rossi, D. H. Son, *J. Am. Chem. Soc.* **2017**, 139, 4358.

[9] Z. Dang, B. Dhanabalan, A. Castelli, R. Dhall, K. C. Bustillo, D. Marchelli, D. Spirito, U. Petralanda, J. Shamsi, L. Manna, R. Krahne, M. P. Arciniegas, *Nano Lett.* **2020**, 20, 1808.

[10] J. A. Steele, M. Lai, Y. Zhang, Z. Lin, J. Hofkens, M. B. J. Roeffaers, P. Yang, *Acc. Mater. Res.* **2020**, 1, 3.

[11] Y. Dong, T. Qiao, D. Kim, D. Parobek, D. Rossi, D. H. Son, *Nano Lett.* **2018**, 18, 3716.

[12] S. Bera, R. K. Behera, N. Pradhan, *J. Am. Chem. Soc.* **2020**, 142, 20865.

[13] N. Pradhan, *Acc. Chem. Res.* **2021**, 54, 1200.

[14] J. Liu, K. Song, Y. Shin, X. Liu, J. Chen, K. Yao, J. Pan, C. Yang, J. Yin, L. Xu, H. Yang, A. M. El-Zohry, B. Xin, S. Mitra, M. N. Hedhili, I. S. Roqan, O. F. Mohammed, Y. Han, O. M. Bakr, *Chem. Mater.* **2019**, 31, 6642.

[15] M. Liu, Q. Wan, H. Wang, F. Carulli, X. Sun, W. Zheng, L. Kong, Q. Zhang, C. Zhang, Q. Zhang, *Nat. Photonics* **2021**, 15, 379.

[16] L. Peng, S. K. Dutta, D. Mondal, B. Hudait, S. Shyamal, R. Xie, P. Mahadevan, N. Pradhan, *J. Am. Chem. Soc.* **2019**, 141, 16160.

[17] A. Haji-Akbari, M. Engel, A. S. Keys, X. Zheng, R. G. Petschek, P. Palffy-Muhoray, S. C. Glotzer, *Nature* **2009**, 462, 773.

[18] T. Chen, Z. Zhang, S. C. Glotzer, *Proc. Natl. Acad. Sci. U.S.A.* **2007**, 104, 717.

[19] D. Zhang, Y. Yang, Y. Bekenstein, Y. Yu, N. A. Gibson, A. B. Wong, S. W. Eaton, N. Kornienko, Q. Kong, M. Lai, A. P. Alivisatos, S. R. Leone, P. Yang, *J. Am. Chem. Soc.* **2016**, 138, 7236.

[20] L. Protesescu, S. Yakunin, M. I. Bodnarchuk, F. Krieg, R. Caputo, C. H. Hendon, R. X. Yang, A. Walsh, M. V. Kovalenko, *Nano Lett.* **2015**, 15, 3692.

[21] G. Jia, A. Sitt, G. B. Hitin, I. Hadar, Y. Bekenstein, Y. Amit, I. Popov, U. Banin, *Nat. Mater.* **2014**, 13, 301.

[22] J. Liu, X. Zheng, O. F. Mohammed, O. M. Bakr, *Acc. Chem. Res.* **2022**, 55, 262.

[23] Q. Zhang, Q. Shang, R. Su, T. T. H. Do, Q. Xiong, *Nano Lett.* **2021**, 21, 1903.

[24] F. Xu, K. Meng, B. Cheng, S. Wang, J. Xu, J. Yu, *Nat. Commun.* **2020**, 11, 4613.

[25] K.-S. Cho, D. V. Talapin, W. Gaschler, C. B. Murray, *J. Am. Chem. Soc.* **2005**, 127, 7140.

[26] F. Xu, X. Ma, L. F. Gerlein, S. G. Cloutier, *Nanotechnology* **2011**, 22, 265604.

[27] B. Hudait, S. K. Dutta, S. Bera, N. Pradhan, *Nano Lett.* **2021**, 21, 5277.

[28] Y.-R. Luo, *Comprehensive handbook of chemical bond energies*, CRC press, 2007.

[29] J. Zhu, Q. Di, X. Zhao, X. Wu, X. Fan, Q. Li, W. Song, Z. Quan, *Inorg. Chem.* **2018**, 57, 6206.

[30] Z. Xiao, K. Z. Du, W. Meng, J. Wang, D. B. Mitzi, Y. Yan, *J. Am. Chem. Soc.* **2017**, 139, 6054.

[31] X. Peng, L. Manna, W. Yang, J. Wickham, E. Scher, A. Kadavanich, A. P. Alivisatos, *Nature* **2000**, 404, 59.

[32] L. Carbone, C. Nobile, M. De Giorgi, F. D. Sala, G. Morello, P. Pompa, M. Hytch, E. Snoeck, A. Fiore, I. R. Franchini, M. Nadasan, A. F. Silvestre, L. Chiodo, S. Kudera, R. Cingolani, R. Krahne, L. Manna, *Nano Lett.* **2007**, 7, 2942.

[33] Y. Yang, C. Hou, T. Liang, *Phys. Chem. Chem. Phys.* **2021**, 23, 7145.

[34] H. H. Fang, F. Wang, S. Adjokatse, N. Zhao, J. Even, M. Antonietta Loi, *Light Sci. Appl.* **2016**, 5, e16056.

[35] J. Xing, F. Yan, Y. Zhao, S. Chen, H. Yu, Q. Zhang, R. Zeng, H. V. Demir, X. Sun, A. Huan, Q. Xiong, *ACS Nano* **2016**, 10, 6623.

[36] S.-T. Ha, C. Shen, J. Zhang, Q. Xiong, *Nat. Photonics* **2016**, 10, 115.

[37] D. Li, G. Wang, H.-C. Cheng, C.-Y. Chen, H. Wu, Y. Liu, Y. Huang, X. Duan, *Nat. Commun.* **2016**, 7, 11330.

[38] Y. Wang, X. Li, J. Song, L. Xiao, H. Zeng, H. Sun, *Adv. Mater.* **2015**, 27, 7101.

[39] J. Chen, W. Du, J. Shi, M. Li, Y. Wang, Q. Zhang, X. Liu, *InfoMat* **2020**, 2, 170.

[40] S. Yakunin, L. Protesescu, F. Krieg, M. I. Bodnarchuk, G. Nedelcu, M. Humer, G. De Luca, M. Fiebig, W. Heiss, M. V. Kovalenko, *Nat. Commun.* **2015**, 6, 8056.

[41] K. Wang, S. Wang, S. Xiao, Q. Song, *Adv. Opt. Mater.* **2018**, 6, 1800278.

[42] M. Sak, N. Taghipour, S. Delikanli, S. Shendre, I. Tanriover, S. Foroutan, Y. Gao, J. Yu, Z. Yanyan, S. Yoo, C. Dang, H. V. Demir, *Adv. Funct. Mater.* **2020**, 30, 1907417.

[43] H. Zhu, Y. Fu, F. Meng, X. Wu, Z. Gong, Q. Ding, M. V. Gustafsson, M. T. Trinh, S. Jin, X. Zhu, *Nat. Mater.* **2015**, 14, 636.

[44] J. Hu, L. Li, W. Yang, L. Manna, L. Wang, A. P. Alivisatos, *Science* **2001**, 292, 2060.

[45] S. N. Raja, Y. Bekenstein, M. A. Koc, S. Fischer, D. Zhang, L. Lin, R. O. Ritchie, P. Yang, A. P. Alivisatos, *ACS Appl. Mater. Inter.* **2016**, 8, 35523.

[46] T. Abir, R. Shechter, T. Ellenbogen, Y. Bekenstein, *ACS Photonics* **2020**, 7, 2329.

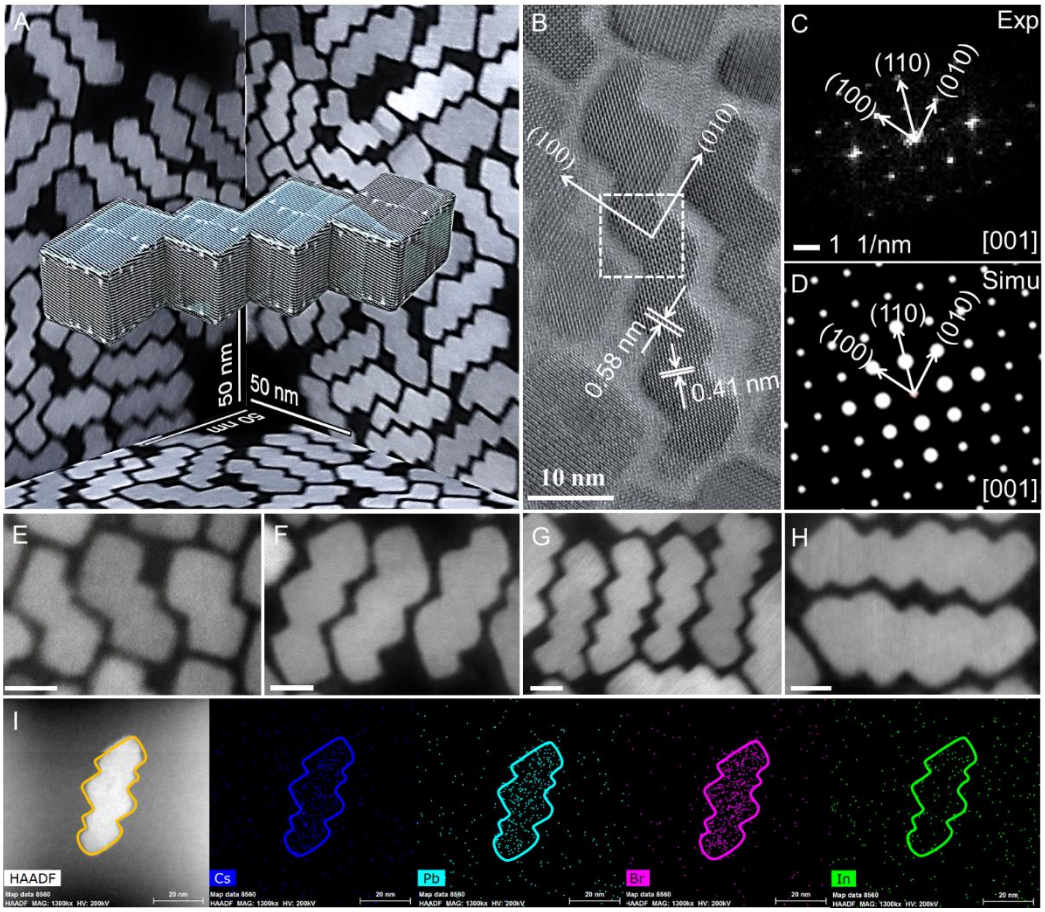

Figure 1 A) Representative HAADF-STEM image and schematic (inset) of zigzag $CsPbBr_3$ nanocrystals with n = 4 (n is the number of nanocube components). **B)** HR-TEM image of zigzag $CsPbBr_3$ nanocrystals. **C)** Fast Fourier Transformed (FFT) patterns of the area indicated by a white box area in B). **D)** Simulated electron diffraction (ED) pattern of the cubic $CsPbBr_3$ structure (space group: Pm-3m (221), PDF card No. 04-007-9893). ED and PDF card No. were acquired using PDF-4+ software version 2009. HAADF-STEM images of zigzag $CsPbBr_3$ nanocrystals with **E)** n = 2, **F)** n = 3, **G)** n = 4, **H)** n > 4. Scale bar in the images is 10 nm. **I)** HAADF-STEM image and elemental maps of an individual zigzag $CsPbBr_3$ nanoparticle.

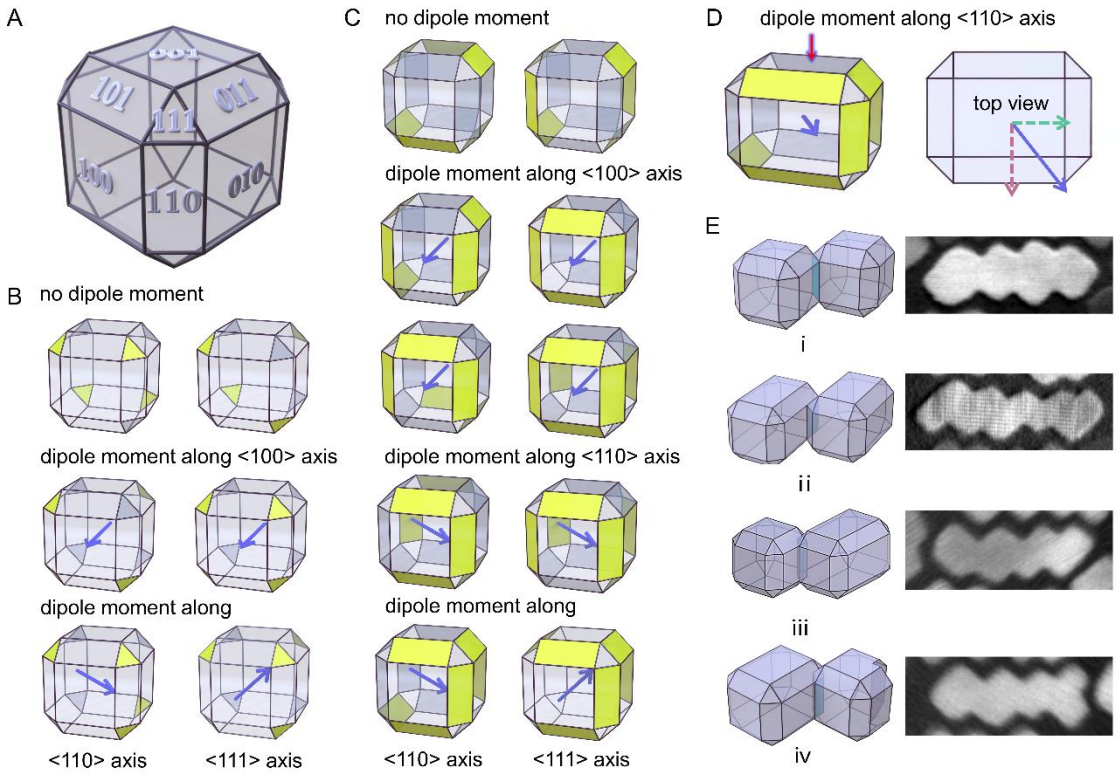

Figure 2 A) Structural models of cubic phase $CsPbBr_3$ nanocrystals; Possible distribution of polar (yellow: negative charged, grey: positive charged) facets and relevant dipole moment direction (blue arrow) attributed to **B)** {111} facets and **C)** {110} facets of ideal cubic $CsPbBr_3$ nanocrystals. **D)** Left: schematic of one of the possible arrangements of rectangular prism shape $CsPbBr_3$ nanocrystal and its dipole moment direction, right: top view of the $CsPbBr_3$ nanocrystal (red and green arrow: direction of component dipole moments generated by {110} polar facets). **E)** Symmetrical (i, ii) and asymmetrical (iii, iv) zigzag $CsPbBr_3$ nanocrystals.

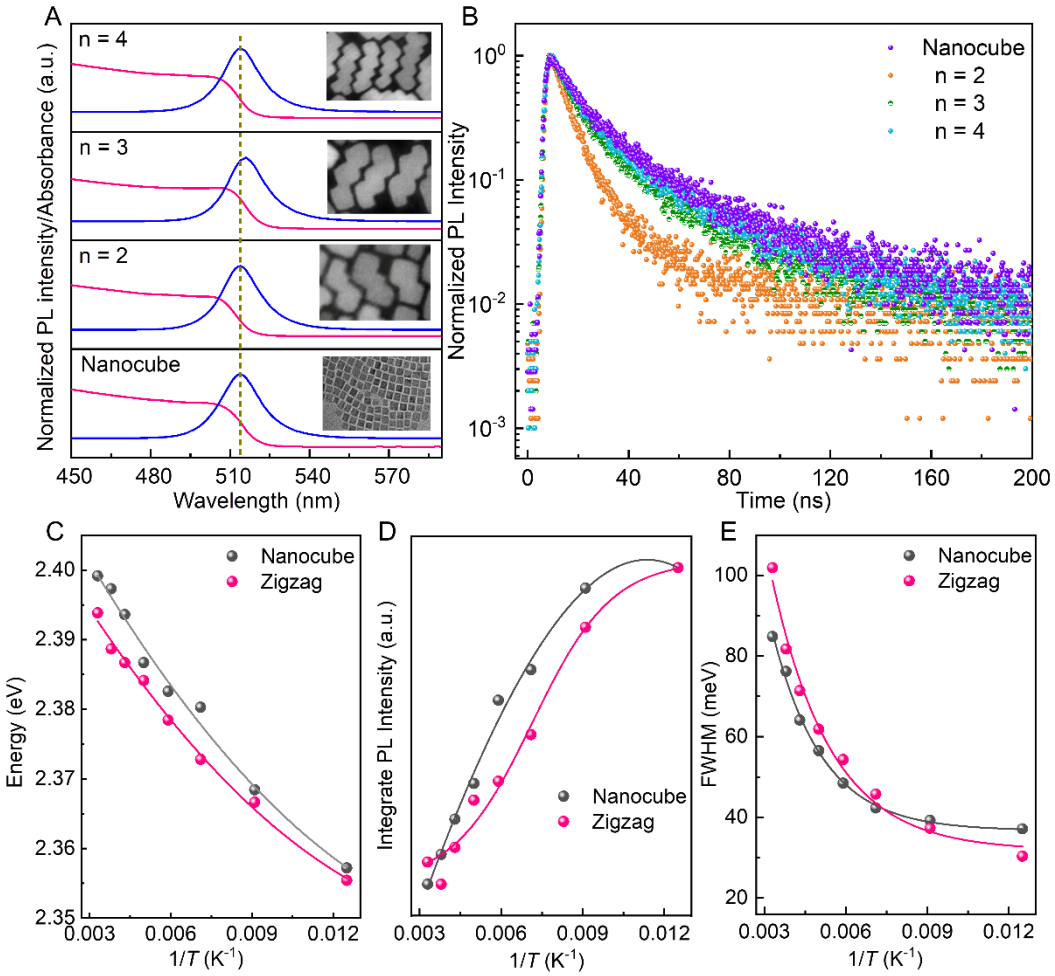

Figure 3 A) UV–vis absorbance and normalized PL spectra and **B)** time-resolved PL decay curves of fresh $CsPbBr_3$ nanocubes and fresh zigzag $CsPbBr_3$ nanocrystals with different number of connections, *n* =2, 3 and 4. Insets show corresponding TEM images. *T*-dependence of **C)** PL peak position, **D)** integrated PL intensity, and **E)** PL linewidth for $CsPbBr_3$ nanocubes and zigzag $CsPbBr_3$ nanocrystals with connections of n = 4. The samples films are excited with λ_{ex} = 350 nm.

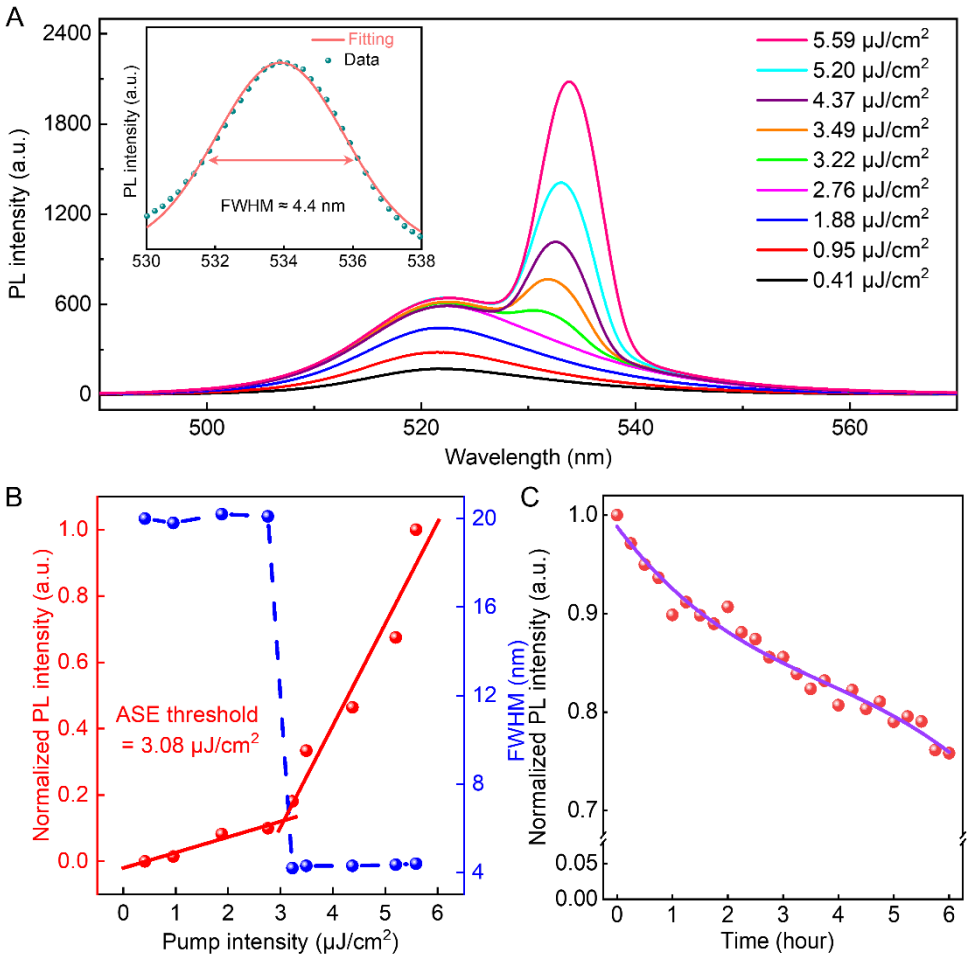

Figure 4 A) Pump intensity-dependent PL spectra from thin film of $CsPbBr_3$ zigzag nanocrystal (n = 4). The inset shows the Gaussian fitting of the ASE peak. **B)** The FWHM of the PL spectra (blue circles) shows abrupt narrowing and the spectrally integrated PL intensity of the sharp peak (red squares) exhibits a threshold behavior with respect to pump intensity. **C)** Plot of stimulated emission peak intensity as a function of pump time (400 nm 1000 Hz femtosecond laser) shows excellent optical stability.

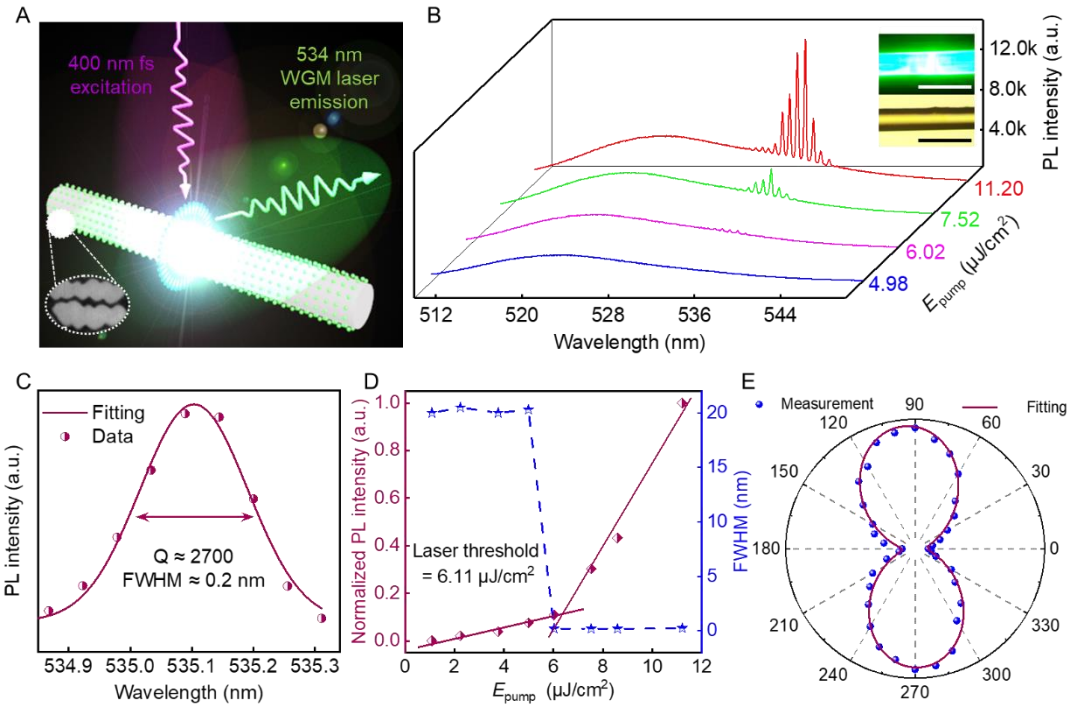

Figure 5 A) Schematic diagram of $CsPbBr_3$ zigzag nanocrystal integrated with a SiO_2 microfiber to form a WGM resonant cavity. **B)** Pump intensity-dependent lasing emission spectra from $CsPbBr_3$ Zigzag nanocrystal. Inset displays the corresponding real-color image of $CsPbBr_3$ zigzag nanocrystal film integrated with a fiber under femtosecond laser excitation (λ_{pump} = 400 nm, 100 fs, 1 kHz). The scale bar is 100 μm. **C)** Gaussian fitting of the lasing peak shows The FWHM of the lasing peaks is 0.2 nm, corresponding Q-factor of about 2700. **D)** Spectrally integrated PL intensity and corresponding FWHM over the lasing peaks with respect to pump intensity. **E)** Polarization-dependent $CsPbBr_3$ zigzag nanocrystal lasing intensities shows high polarization state (R = 0.80).

The table of contents entry:

Zigzag $CsPbBr_3$ perovskite nanocrystals with a precise number of nanocube are synthesized through a dipole-induced self-assembly process. Dipole moment along <110> axis is found to be the driving force for the assembly of nanocubes into zigzag nanocrystals. The zigzag $CsPbBr_3$ nanocrystals exhibit desirable optical properties comparable to their nanocube counterparts and offer advantages for amplified spontaneous emission (ASE) and lasing applications with low pump thresholds of 3.1 μJ/cm^2 and 6.02 μJ/cm^2, respectively.

Keywords: zigzag perovskite nanocrystals, dipole-induced self-assembly, optical properties, amplified spontaneous emission, lasing

Authors: C. Zhang, J. Chen, L. Turyanska, J. Wang, W. Wang, L. Wang, L. Kong, K. Wu, J. Yao, H. Yao, Z. Yang, W. Li, Y. Bekenstein, Y. Wang,* G. Jia,* and X. Yang*

Title: Highly Controlled Zigzag Perovskite Nanocrystals Enabled by Dipole-induced Self-Assembly of Nanocubes for Low-threshold Amplified Spontaneous Emission and Lasing

TOC Figure